Mem. S.A.It. Vol. 91, 311

**Memorie** della


# Turbulence and magnetic reconnection in low-beta plasmas

L. Franci[1,2] and E. Papini[3,2]

[1] School of Physics and Astronomy, Queen Mary University of London, 327 Mile End Road, E1 4NS, London, UK, e-mail: l.franci@qmul.ac.uk
[2] Istituto Nazionale di Astrofisica, Osservatorio Astrofisico di Arcetri, Largo E. Fermi 5, 50125, Firenze, Italy
[3] Dipartimento di Fisica e Astronomia, Università degli Studi di Firenze, Via G. Sansone 1, 50019, Sesto Fiorentino, Italy

**Abstract.** Understanding how the turbulent energy cascade terminates at small scales in collisionless plasmas represents a long-standing challenge for the plasma community, and is strictly related to the open issues of coronal heating and solar wind heating and acceleration. Here we investigate the dynamics of low-beta turbulent plasmas by performing high-resolution 2D and 3D hybrid particle-in-cell simulations of the near-Sun environment. Our aim is to infer how the low plasma beta, typical of the solar corona, affects the development and properties of turbulence and magnetic reconnection and their interplay. We indeed identify a new plasma regime at ion characteristic scales. Such regime has different properties of the electromagnetic and plasma fluctuations with respect to what is typically observed in the solar wind and in the Earth's magnetosheath. A stronger activity of magnetic reconnection is also observed. We expect that such regime may be relevant for a broad class of low-beta plasmas, both in space, astrophysical, and laboratory environments.

**Key words.** Plasmas – Turbulence – Magnetic reconnection – Solar wind

## 1. Introduction

Plasmas represent the most abundant form of ordinary matter in the Universe and usually exist in a turbulent state. As a consequence, plasma turbulence is a widespread and ubiquitous phenomenon, observed in many different space and astrophysical environments. These include, among others, the solar wind (e.g. Verscharen et al. 2019), the Earth's magnetosphere (e.g. Chen & Boldyrev 2017), galaxy clusters (e.g. Roncarelli et al. 2018), and the interstellar medium (e.g. Burkert 2006). In-situ spacecraft observations of the solar wind and the near-Earth environment from both field and particle instruments show power spectra of fluctuations which exhibit a power-law behavior spanning several decades in frequency (Kiyani et al. 2015). This is typically interpreted as the signature of a "turbulent energy cascade": the energy is transferred from large magnetohydrodynamic (MHD) scales, where it is injected, to small kinetic scales (i.e., scales comparable to the ion and electron gyroradii), where it is dissipated.

Although plasma turbulence has been deeply investigated for decades by means of theoretical models, in situ observations, and

numerical simulations, many aspects of how the cascade operates still represent an open issue, especially at kinetic scales. In the solar wind plasma, due to its very low density, collisions between particles are rare, thus they cannot represent an efficient mechanism for energy dissipation. A long-standing challenge for the plasma community is therefore understanding how, in the absence of a collisional viscosity, the turbulent cascade terminates at small scales. Possible candidate mechanisms for energy dissipation at small kinetic scales include the nonlinear interaction of dispersive wave modes and magnetic reconnection.

Here we present recent results from high-resolution 2D and 3D hybrid particle-in-cell direct numerical simulations (DNS) that provide new insights for interpreting observational data from past and present spacecraft missions. Our DNS recover an unprecedented agreement with observational results, but their importance is not limited to this. They also provide additional information that cannot be available from single (or even multi) spacecraft observations, such as e.g., a full characterization of the spatiotemporal dynamics and a clear visualization of the physical structures and their shape and size.

More in general, they provide simultaneous measurements of both the electromagnetic and plasma fluctuations in several points in space and time and with high enough accuracy to capture the dynamics at kinetic scales (unlike in observations, where high-resolution measurements of all the relevant fields are usually not available, due to telemetry constraints and/or instrumental capabilities). The support from numerical modelling is therefore fundamental for a comprehensive analysis and understanding of the plasma dynamics. For this reason, our study is of great relevance for the space physics and plasma communities, among which kinetic-scale turbulence and its direct link with magnetic reconnection are currently hot topics (e.g. Matthaeus & Velli 2011).

## 2. Simulations of low-beta plasmas

### 2.1. Numerical code and setup

The DNS have been performed using the hybrid particle-in-cell code CAMELIA on Marconi-A2 at the Italian SuperComputing centre CINECA. CAMELIA is based on the Current Advance Method and Cyclic Leapfrog (CAM-CL) code of Matthews (Matthews 1994) and solves the Vlasov-Maxwell equations, comprising the equations of motions for individual ions, and the electron fluid equations. The code employs a hybrid approach. On one hand, the ions are modelled as macroparticles, i.e., fluid elements representing portions of the particles velocity distribution functions (VDF) in phase space, and are tracked in a Lagrangian frame, whereas moments of the VDF, such as densities and currents, are computed simultaneously on Eulerian (fixed) mesh points. On the other hand, electrons act as a massless, isothermal, and charge-neutralizing fluid.

CAMELIA has been ported and run with optimal performance on many HPC systems with different architectures. An example of the code performance on Marconi-A2 is shown in Fig. 1 for with three different sizes. Further information on the computational method, the model equations, as well as the code performance can be found in Franci et al. (2018).

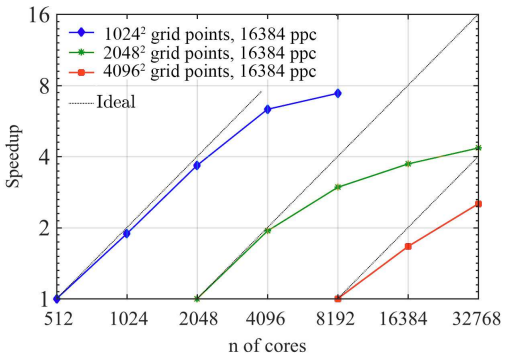


**Fig. 1.** Strong scaling performance of the hybrid particle-in-cell code CAMELIA on the Marconi-A2 HPC system at the Italian SuperComputing centre CINECA.

**Table 1.** List of DNS and their main physical and numerical parameters. From left to right: DNS name, number of grid points, size of the computational box, spatial resolution, wavenumber corresponding to the energy injection scale, initial level of magnetic fluctuations, ion and electron beta, number of particles per cell, and references where the DNS are analysed in detail.

| Name | Grid | $L\,(d_i)$ | $\delta\,(d_i)$ | $k^{\rm inj}\,(d_i^{-1})$ | $\mathbf{B}^{\rm rms}\,(B_0)$ | $\beta_i$ | $\beta_e$ | ppc | References |
|---|---|---|---|---|---|---|---|---|---|
| DNS1 | $4096^2$ | 256 | 1/16 | 0.4 | 0.44 | 0.2 | 0.5 | 1024 | Franci et al. (2020a) |
| DNS2 | $512^3$ | 64 | 1/8 | 0.5 | 0.33 | 0.2 | 0.5 | 512 | Franci et al. (2020a) |
| DNS3 | $2048^2$ | 256 | 1/8 | 0.28 | 0.24 | 0.5 | 0.5 | 8000 | Franci et al. (2015a,b) |

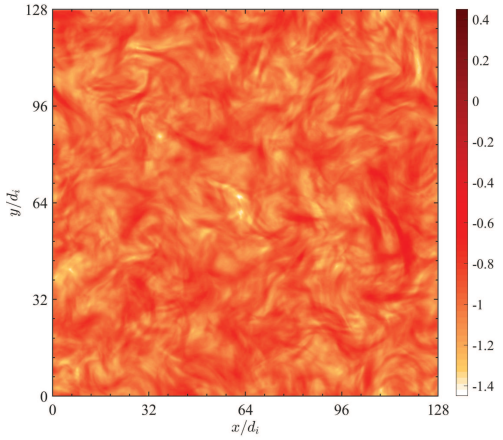


**Fig. 2.** Contour plot of the common logarithm of the squared magnitude of the magnetic fluctuations of DNS2, integrated along the direction of the ambient magnetic field.

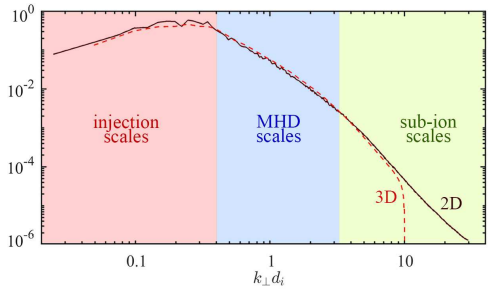


**Fig. 3.** Comparison of the 1D power spectum of the magnetic field for the 2D simulation DNS1 (dark red solid line) and the 3D simulation DNS2 (red dashed line) The injection, MHD, and sub-ion scales are also marked with different colors.

Here we present results from three DNS performed in the low-plasma beta regime, where the ion (electron) plasma beta $\beta_{i,e} = 8\pi P_{i,e}/B_0^2$ is the ratio between the ion (electron) pressure and the pressure of the ambient magnetic field $B_0$. The first two runs are from a $4096^2$ and from a $512^3$ hybrid DNS, which we call DNS1 and DNS2 respectively. These results were recently presented in Franci et al. (2018). We also compare DNS1 with a 2D DNS from our previous studies (Franci et al. 2015a,b), which we refer to as DNS3. The initial condition for all the DNS consists of a homogeneous plasma embedded in a uniform ambient magnetic field, $\mathbf{B}_0 = B_0\hat{\mathbf{z}}$, which in the 2D case is out of the $(x, y)$ simulation plane. We perturb the plasma with Alfvénic-like magnetic and ion bulk velocity fluctuations perpendicular to $\mathbf{B}_0$. Such fluctuations results from the superposition of Fourier modes of wavenumber $k \leq k^{\rm inj}$, with same amplitude and different random phases, and with energy equipartition between magnetic and kinetic energy. The physical and numerical parameters for each DNS are summarized in Tab. 1 and further discussed in the related references. The magnetic field is expressed in units of the magnitude of the ambient magnetic field, $B_0$, the ion bulk velocity is in units of the Alfvén velocity, $V_A$, time is in units of inverse ion gyrofrequency, $\Omega_{\rm i}^{-1}$, and lengths are in units of the ion inertial length, $d_{\rm i} = V_A/\Omega_{\rm i}$.

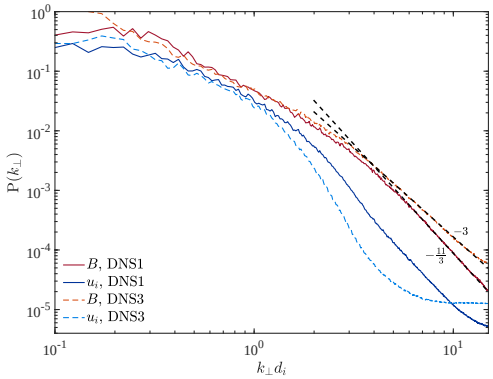


**Fig. 4.** Power spectra of the magnetic field (tones of red) and of the the ion bulk velocity (tones of blue) for DNS1 (solid) and DNS3 (dashed).

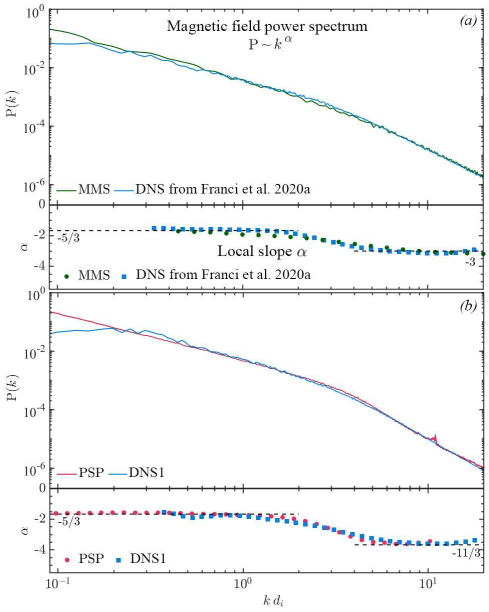


**Fig. 5.** Direct comparison of the magnetic field spectrum between our DNS and spacecraft observations by MMS (a) and PSP (b), in the near-Earth and in the near-Sun environment, respectively.

## 2.2. Spectral properties of turbulence

We let the plasma evolve until turbulence has fully developed and reached an almost stationary state. This correspond to the time when the rms value of the current density, $\mathbf{J} = \nabla \times \mathbf{B}$, attains a maximum followed by a plateau (Mininni & Pouquet 2009). An example of how the system looks like at the time of maximum turbulent activity is provided in Fig. 2 for DNS2. Here we show the squared magnitude of the magnetic fluctuations integrated along the direction of the ambient magnetic field, which is orthogonal to the $xy$-plane. The same quantity (not integrated) in the whole 3D domain for DNS2 and in the whole 2D domain for DNS1 is shown in Franci et al. (2020a).

The corresponding 1D isotropized power spectrum of the magnetic field for the two DNS are compared in Fig. 3. We clearly see that the power spectra are qualitatively and quantitatively the same, regardless of the geometry (2D and 3D respectively) of the simulation domain (cf. also Franci et al. 2018). Here we take the chance to highlight different ranges in the wavenumber domain: (i) the red shaded region marks the injection scales, where the energy is injected; (ii) the blue shaded region corresponds to the so called magnetohydrodynamic (MHD) intertial range, where a power law with a slope (spectral index) of $-5/3$ is usually observed; (iii) the green shaded region corresponds to what are typically called the sub-ion scales in the sense that they are smaller than the ion characteristic scales, i.e., the ion inertial length, $d_i$, and the ion gyroradius, $\rho_i = \sqrt{\beta_i}/, d_i$. In this third region, the magnetic field spectrum is always observed to steepen, although the spectral index may vary.

In Fig. 4, we compare the power spectra of the magnetic field, $B$, and of the ion bulk velocity, $u_i$, for simulations DNS1 and DNS3. We recall that, as shown in Tab. 1, these two DNS are quite similar to each other as far as the main physical parameters are concerned. The two main differences are the value of the ion plasma beta (a factor of 2.5 between the two) and the level of initial magnetic fluctuations (a factor of $\sim$ 2). We observe a good agreement between the two DNS for both $B$ and $u_i$ at MHD scales. The spectral behavior, however, is quite different at sub ion scales. The magnetic field spectrum has a spectral index of $-11/3$ in DNS1 and $-3$ in DNS3. The latter is closer to the value measured on average in both observations and DNS of plasma turbu-

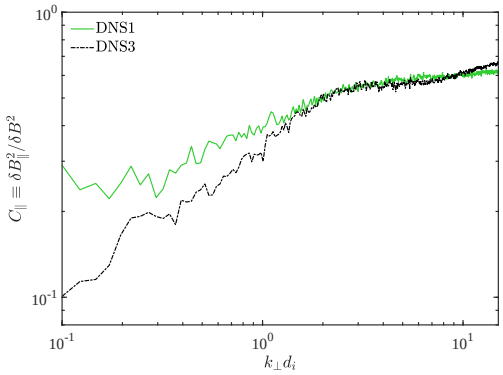


**Fig. 6.** Magnetic compressibility, $C_\parallel$, in DNS1 (solid green) and DNS3 (dot-dashed black).

lence in the solar wind and at the Earth's magnetopause (e.g., Matteini et al. 2020; Franci et al. 2020b), while the former is compatible with what has been recently observed closer to the Sun by the Parker Solar Probe (PSP) spacecraft (e.g., Bowen et al. 2020; Franci et al. 2020a). Even the velocity spectrum differs, as the level of the fluctuations starts decreasing at a slightly larger scale for DNS3, consistently with the fact that the ion gyroradius is about a factor of $\sim 1.5$ larger than for DNS1. Another major difference is that in DNS3 the velocity spectrum drops down quite steep, until the noise level is reached. In DNS1, on the contrary, it exhibits a power-law behavior with a slope comparable to the one of the magnetic field spectrum. More importantly, the ratio between the spectrum of $B$ and the spectrum of $u_i$ is quite larger for DNS1 than for DNS3. As a consequence, the ion kinetic energy provides a non-negligible contribution to the total energy at sub-ion scales in the latter but not in the former. This determines the occurrence of a different plasma regime, as we recently discussed in Franci et al. (2020a).

The magnetic field spectrum of DNS1 is found to be in very good agreement with observations by the PSP spacecraft at its first perihelion, corresponding to a distance from the Sun of 35.7 solar radii, as shown in Fig. 5b. This is not the first time that our DNS recover a remarkable agreement with observational data, as we recently also reproduced the magnetic field power spectrum obtained from measurements by the Magnetospheric Multiscale (MMS) spacecraft mission at the Earht's magnetopause (see Fig. 5a).

Recently we have also investigated the magnetic compressibility, i.e., the ratio of the power in the parallel (with respect to the ambient magnetic field) magnetic fluctuations to the power of the total magnetic fluctuations $C_\parallel = \delta B_\parallel^2/\delta B^2$, by comparing our hybrid DNS with solar wind observations (Matteini et al. 2020). In Fig. 6 we show the magnetic compressibility of DNS1 and DNS3. They are different at MHD scales, likely related to the different initial level of turbulent fluctuations, as already been observed in our previous DNS (e.g., Franci et al. 2018). Despite this, the two DNS exhibit almost the same level of magnetic compressibility at sub-ion scales, as this is strictly related to the physical plasma conditions, regardless of the slope of the magnetic field spectrum.

## 2.3. Magnetic reconnection

Plasma instabilities can provide very efficient channels for the dissipation of magnetic energy throughout the turbulent cascade. In particular, magnetic reconnection taking place in current sheets (CS) arises as one of the most prominent instabilities in plasma environments (e.g. Matthaeus & Velli 2011). A critical quantity that allows to assess the interplay between magnetic reconnection and turbulence is the reconnection rate, which gives the characteristic time needed by reconnection to reprocess the large-scale magnetic energy entering the CS into magnetic, internal, and kinetic energy.

In Fig. 7, we report the distribution of the reconnection rates measured in DNS1, as the system evolves from its initial configuration toward a fully developed turbulent state. The first reconnection events are triggered at the edges of the largest turbulent eddies that form as a result of the initial relaxation, at around $t = 10\,\Omega_i^{-1}$, i.e. much before the maximum of turbulent activity is reached (at $t = 50\,\Omega_i^{-1}$). In between the eddies, thin elongated CS form spontaneously and then become tearing unsta-

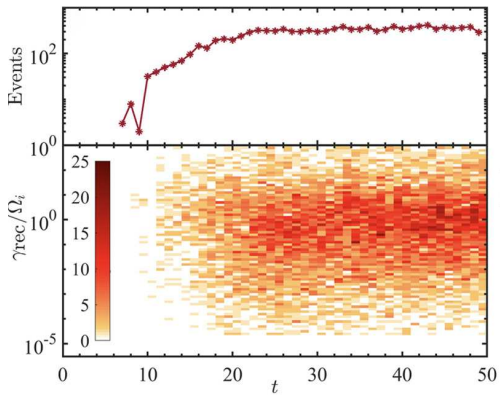


**Fig. 7.** Time evolution of magnetic reconnection events is DNS1. Top panel: number of total events in the simulation domain. Bottom panel: reconnection rate $\gamma_{\rm rec}/\Omega_i$. The procedure for automatically detecting the events and for computing their reconnection rate is described in Papini et al. (2019b).

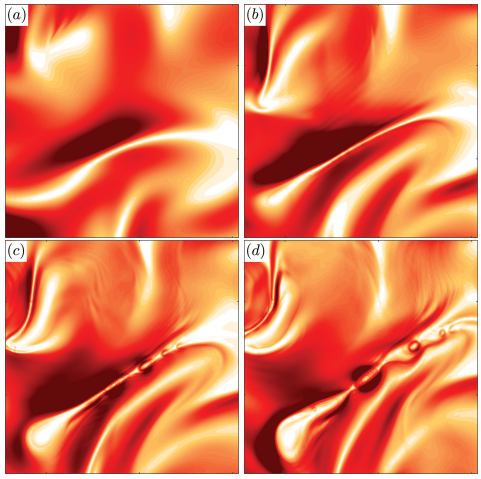


**Fig. 8.** Contour plot of the squared magnitude of the magnetic fluctuations perpendicular to the ambient magnetic field in a $32d_i \times 32d_i$ zoomed region of DNS1. The different phases of the evolution of a current sheet undergoing magnetic reconnection are shown. The current sheet forms at $t \sim 10\,\Omega_i^{-1}$ (a) and gets squeezed until $t \sim 20\,\Omega_i^{-1}$ (b). Reconnection starts occurring and small plasmoids form at $t \sim 25\,\Omega_i^{-1}$ (c), which then grow in size and are ejected away from the current sheet. As a consequence, this get disrupted at $t \sim 30\,\Omega_i^{-1}$ (d).

ble (Furth et al. 1963). A fast Hall-plasmoid instability then develops (Papini et al. 2019c), which ultimately brings to the disruption of the CS and to the expulsion of plasmoids of size of few inertial lengths $d_i$ in the turbulent surroundings. As an example, Fig. 8 show the evolution of magnetic reconnection in one of the many CS that are found in DNS1. The number of reconnection events (top panel of Fig. 7) then rapidly increases and, after a short transient phase, becomes roughly constant. Concurrently, the distribution of the reconnection rates (bottom panel) also becomes quite constant in time, meaning that reconnection events are statistically stationary. The average reconnection rate is $\gamma_{\rm rec}/\Omega_i \sim 10$, which denotes a characteristic reconnection time much shorter than the eddy turnover time. Such results, in agreement with what has been found in our previous DNS (Papini et al. 2019a,b), support the existence of a reconnection-mediated turbulence regime in DNS1, in which magnetic reconnection provides a direct channel to drive the turbulence at sub-ion scales (Franci et al. 2017).

## 2.4. Multiscale analysis

The different ranges we highlighted in Fig. 3, identified by the changing behavior of the magnetic field power spectrum, reveal the intrinsic multiscale nature of turbulence. Spectral methods allow to carefully characterize the global properties of turbulent plasmas. They are, however, not capable to isolate the contribution of localized magnetic structures, because the information about the spatial localization of features is lost in the spectral decomposition.

To overcome this issue, we recently performed a multiscale analysis of DNS of plasma turbulence (Papini et al. 2020), by employing Multidimensional Iterative Filtering (MIF), a new powerful technique for the analysis of nonstationary nonlinear multidimensional signals (Cicone & Zhou 2017). Given a multidimensional field, MIF decomposes it into a finite number of simple oscillating components called Intrinsic Mode Functions (IMF)

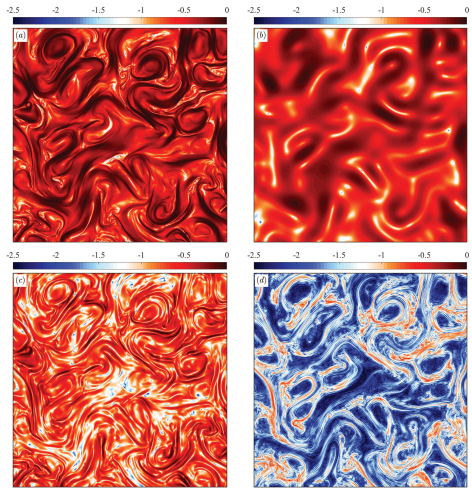

**Fig. 9.** Contour plot of the common logarithm of the magnitude of magnetic fluctuations of DNS1 in the whole range of scales (a) and at the injection (b), MHD (c), and sub-ion (d) scales, as obtained with the MIF analysis. For the sake of clarity, we show here only 1/4 of the simulation domain.

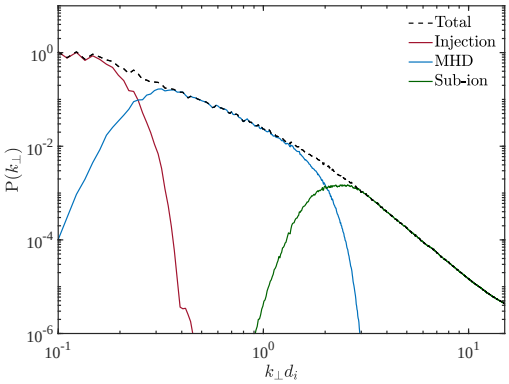


**Fig. 10.** Power spectrum of the magnetic field for DNS1 (black), and power spectra of the fields obtained from the MIF decomposition (See Fig. 9) at injection (red), MHD (blue), and sub-ion scales (green).

whose average wavenumber is well-behaved. Such decomposition is adaptive, based on the local characteristic scales of the field, and with no constraint on the shape of the features to be extracted.

Using MIF, we performed a multiscale analysis of DNS1 and isolated the magnetic field contribution to the turbulent cascade in the three different ranges of scales (injection, MHD, and ion-kinetic) previously identified (for more details on the analysis see Papini et al. 2020). Fig. 9 shows the magnitude of the turbulent magnetic fluctuations in such ranges. The injection-scale component, remnant of the initial condition, fills the space almost uniformly (top-right panel). The MHD component (bottom-left) contains the large turbulent eddies and, between them, the large-scale background magnetic field configuration of the current sheets. Finally, the sub-ion scales component reveals very localized magnetic features, organized in a filamented network at the edge of the turbulent eddies.

Finally, in Fig. 10 we report the 1D Power spectrum of the total magnetic field fluctuations of DNS1, already shown in Fig. 3, together with the power spectra obtained by the decomposed contributions shown in Fig. 9. The injection, MHD, and sub-ion ranges are well separated, which confirms the ability of the MIF decomposition to isolate the different scales, while retaining the full spatial information of the fields.

## 3. Conclusions

Our new high-resolution 2D and 3D DNS of low-beta plasmas provided the first numerical evidence of a new turbulent regime at scales just below the ion inertial length. Our results are in quantitative agreeement with observational evidence from in situ measurement of the near-Sun environment by the PSP spacecraft. These new DNS exhibit a few interesting differences with respect to our previous DNS (e.g., DNS3), which showed a behavior more typical of the solar wind plasma and of the near-Earth environment. These include different spectral properties at sub-ion scales (e.g., a steeper magnetic field spectrum and a larger level of ion bulk velocity fluctuations, despite the same level of magnetic compressibility), and a stronger role of magnetic reconnection (e.g., a larger number of events and a much larger reconnection rate) with respect to what is typically observed in plasmas with a larger beta (Franci et al. 2017; Papini et al. 2019b).

Further analysis and additional simulations are ongoing in order to fully characterize the properties of this newly observed turbulent plasma regime and the required physical conditions, following our recent work (Franci et al. 2020a; Franci & Del Sarto 2020).

*Acknowledgements.* We thank all the coauthors of the publications that include simulations produced using the computing allocation mentioned below: D. Del Sarto, P. Hellinger, D. Burgess, A. Giroul, S. D. Bale, S. Landi, L. Matteini, A. Verdini, O. Alexadrova, C. Lacombe, A. Cicone, and M. Piersanti. L.F. is supported by the UK Science and Technology Facilities Council (STFC) grants ST/P000622/1 and ST/T00018X/1. We acknowledge Istituto Nazionale di Astrofisica (INAF) and CINECA for the availability of high performance computing resources and support under the program "Accordo Quadro MoU per lo svolgimento di attività congiunta di ricerca Nuove frontiere in Astrofisica: HPC e Data Exploration di nuova generazione" (grant C4A26). This resource allocation was used to perform simulations and/or analysis that are presented in Franci et al. (2020b,a); Franci & Del Sarto (2020); Matteini et al. (2020); Papini et al. (2020), where it has therefore been acknowledged.

## References

Bowen, T. A., Mallet, A., Bale, S. D., et al. 2020, Phys. Rev. Lett., 125, 025102
Burkert, A. 2006, C. R. Phys., 7, 433
Chen, C. H. K. & Boldyrev, S. 2017, ApJ, 842, 122
Cicone, A. & Zhou, H. 2017, Numer. Math., 10, 278
Franci, L., et al. 2015a, ApJ, 812, 21
Franci, L., et al. 2015b, ApJ, 804, L39
Franci, L., Cerri, S. S., Califano, F., et al. 2017, ApJ, 850, L16
Franci, L., Hellinger, P., Guarrasi, M., et al. 2018, J. Phys. Conf. Ser., 1031, 012002
Franci, L. & Del Sarto, D. 2020, to be submitted
Franci, L., Del Sarto, D., Papini, E., et al. 2020a, arXiv e-prints, arXiv:2010.05048
Franci, L., Stawarz, J. E., Papini, E., et al. 2020b, ApJ, 898, 175
Furth, H. P., Killeen, J., & Rosenbluth, M. N. 1963, Physics of Fluids, 6, 459
Kiyani, K. H., Osman, K. T., & Chapman, S. C. 2015, Philos. Trans. Royal Soc. A, 373, 20140155
Matteini, L., Franci, L., Alexandrova, O., et al. 2020, Front. Astron. Space Sci., arXiv:2008.13219, in press
Matthaeus, W. H. & Velli, M. 2011, Space Sci. Rev., 160, 145
Matthews, A. P. 1994, J. Comput. Phys., 112, 102
Mininni, P. D. & Pouquet, A. 2009, Phys. Rev. E, 80, 025401
Papini, E., Franci, L., Landi, S., et al. 2019a, Nuovo Cimento C, 42, 23
Papini, E., Franci, L., Landi, S., et al. 2019b, ApJ, 870, 52
Papini, E., Landi, S., & Del Zanna, L. 2019c, ApJ, 885, 56
Papini, E., Cicone, A., Piersanti, M., et al. 2020, J. Plasma Phys., 86, 871860501
Roncarelli, M., Gaspari, M., Ettori, S., et al. 2018, A&A, 618, A39
Verscharen, D., Klein, K. G., & Maruca, B. A. 2019, Living Rev. Sol. Phys., 16, 5